


Femtosecond Laser-Inscribed High-Order Bragg Gratings in Large-Diameter Sapphire Fibers for High-Temperature and Strain Sensing

Chao Chen , Xuan-Yu Zhang, Yong-Sen Yu, Wei-Hua Wei, Qi Guo, Li Qin, Yong-Qiang Ning, Li-Jun Wang, and Hong-Bo Sun , *Fellow, IEEE*

Abstract—Aiming for structural health monitoring applications in harsh environments, a high-order sapphire fiber Bragg grating (HO-SFBG) written with a femtosecond (fs) laser in a large-diameter sapphire fiber is demonstrated. The radial refractive index modulation area induced by scanning exposure is greater than 60% of the fiber cross-section area. The large mode overlapping area leads to a transmission resonance strength of approximately 3.0 dB. As demonstrated by numerical simulations of mode excitation and multimode resonance, each mode resonance is significantly superposed when the coupling coefficient is above 0.0005. A study of the high-temperature and strain sensing characteristics of the HO-SFBG shows that each high-order resonance has different response characteristics. This type of large-diameter SFBG has important application potential for high-temperature smart materials with embedded fiber sensors.

Index Terms—Femtosecond (fs) laser, fiber Bragg gratings, optical fiber sensors, sapphire fiber.

I. INTRODUCTION

SINGLE-CRYSTAL sapphire fibers (SFs) are an ideal material for fiber sensing under harsh conditions, such as high temperature, high pressure, and strong radiation, because of the notable advantages of high melting point (2053 °C), high mechanical strength (the rigidity and Young's modulus of sap-

phire are 7 and 5 times larger than those of silica, respectively), and strong corrosion resistance of SFs compared with silica fibers [1]. SFs have great application potential in structural health monitoring for turbine engines [2], aerospace vehicles [3], and nuclear reactors [4]. The high-temperature components and protective layers of these devices, such as the combustion chamber wall, turbine blade, and skin, are primarily composed of high-temperature resistant materials such as alloy, ceramic, and intermetallic compounds. Achieving anti-electromagnetic interference and multiplexing intelligent sensing networks by embedding fiber sensors [5], [6] in these devices is the most promising scheme for manufacturing 3D intelligent composite materials and for realizing nondestructive testing [7], [8]. To date, it has been reported that SFs can be embedded in NiAl material to build an intermetallic compound-based composite material, with the aim to enhance the room temperature tenacity, thermal shock resistance, creep resistance, and high-temperature mechanical strength of the intermetallic compound [9]. More importantly, large-diameter SFs have a strong ability to enhance composite materials. For optical sensing, we should also consider the light transmission efficiency of embedded SFs. Ghazanfari *et al.* successfully embedded a SF sensor in the fabrication process of Al₂O₃ ceramic components [10] and demonstrated that the transmissivity of a 250- μ m-diameter SF was 56%, which was bearable for sensing applications.

For an embedded fiber sensor with multiplexing and distributed sensing abilities, fiber Bragg grating (FBG) is superior to fiber Fabry-Perot interferometer [5], [6], [11]. The writing of Bragg grating in SF is accompanied by the development of ultrafast laser fabrication technology [12]–[14]. Grobnc *et al.* were the first to demonstrate a multimode sapphire FBG (SFBG) written with a femtosecond (fs) laser and tested its high-temperature stability up to 1500 °C [15]. Elsmann *et al.* inscribed a first-order Bragg grating with a 400-nm fs laser and a Talbot interferometer and demonstrated the functionality of a three-grating multiplexing sensor [16]. Previous reports have primarily focused on SFBGs with a diameter ≤ 150 μ m, because the researchers pay more attention to the effects of multimode transmission [17]–[20]. At the same time, there have been few numerical simulation reports regarding the multimode excitation and multimode resonance characteristics of SFBGs. Thus far, the only related report is that of Zhan *et al.*, who analysed the effective

Manuscript received September 16, 2017; revised December 30, 2017, March 23, 2018, and May 4, 2018; accepted May 21, 2018. Date of publication May 25, 2018; date of current version June 19, 2018. This work was supported in part by the National Science and Technology Major Project of China under Grant 2016YFE0126800, in part by the National Natural Science Foundation of China under Grants 61505206, 61674148, and 61727822, in part by the Science and Technology Development Project of Jilin Province under Grant 20180201014GX, and in part by the Frontier Science Key Program of President of the Chinese Academy of Sciences under Grant QYZDY-SSW-JSC006. (Corresponding authors: Yong-Sen Yu and Hong-Bo Sun.)

C. Chen, L. Qin, Y.-Q. Ning, and L.-J. Wang are with the State Key Laboratory of Luminescence and Application, Changchun Institute of Optics, Fine Mechanics and Physics, Chinese Academy of Sciences, Changchun 130033, China (e-mail: chenc@ciomp.ac.cn).

X.-Y. Zhang, Y.-S. Yu, W.-H. Wei, and Q. Guo are with the State Key Laboratory on Integrated Optoelectronics, College of Electronic Science and Engineering, Jilin University, Changchun 130012, China (e-mail: yuys@jlu.edu.cn).

H.-B. Sun is with the State Key Laboratory on Integrated Optoelectronics, College of Electronic Science and Engineering, Jilin University, Changchun 130012, China, and also with the State Key Laboratory of Precision Measurement and Instruments, Department of Precision Instrument, Tsinghua University, Beijing 100084, China (e-mail: hbsun@tsinghua.edu.cn).

Color versions of one or more of the figures in this paper are available online at <http://ieeexplore.ieee.org>.

Digital Object Identifier 10.1109/JLT.2018.2840699

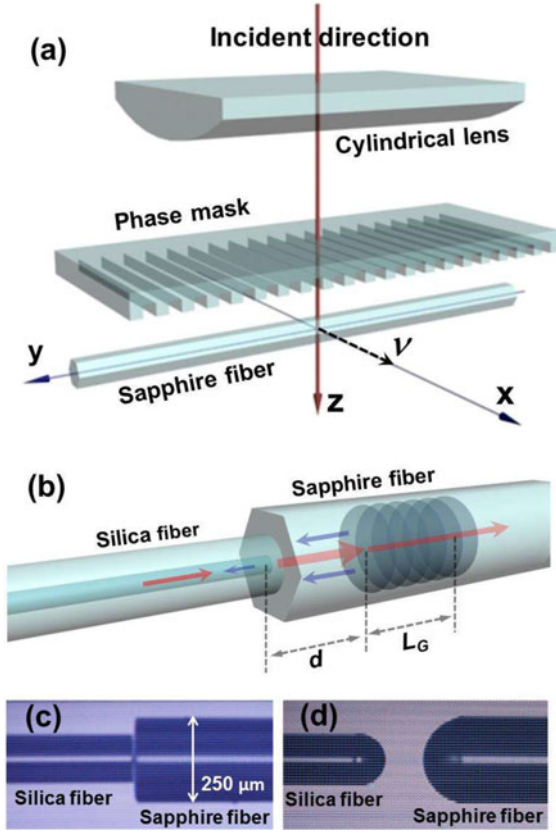


Fig. 1. (a) Schematic of the HO-SFBG written by an fs laser. Schematic (b) and microscopy image (c) of the splicing coupling structure between the SF with a Bragg grating and the MMF. (d) Microscopy image of coupling with the micro-lens.

refractive index (RI) of 25 guided modes in a SF with a diameter of 70 μm based on mode dispersion relationships [19].

Therefore, for applications of structural health monitoring in harsh environments, a high-order SFBG (HO-SFBG) written by an fs laser scanning exposure method in large-diameter (250 μm) SFs is demonstrated in this paper. The induced radial RI change covers 60% of the total fiber cross-section area, and the large mode overlapping area leads to a transmission resonance strength of approximately 3.0 dB. Using numerical simulations of the multimode resonance, we demonstrate that the resonance of each mode will be significantly superposed when the coupling coefficient is larger than 0.0005. We also study the high-temperature and strain sensing characteristics of the 4th- and 5th-order Bragg resonances and discussed the temperature-strain cross-sensitivity problem and possible solutions at the present stage.

II. EXPERIMENTAL METHODS

A. Fs Laser-Inscribed High-Order Bragg Gratings in a SF

The schematic of the fs laser scanning exposure writing setup of the large-diameter SFBG is shown in Fig. 1(a). A Ti:sapphire regenerative amplified laser system (Spectra Physics) with an operation wavelength of $\lambda_{in} = 800$ nm and a pulse duration of 100 fs is used. The pulse repetition rate and pulse energy

are 100 Hz and 0.45 mJ/pulse, respectively. A beam with a radius $\omega_0 = 2.5$ mm is incident on the SF after passing through a cylindrical lens (focal length, $f = 40$ mm) and phase mask (period, $\Lambda_{pm} = 3.33$ μm). The SF was manufactured by Photran, Inc. with a diameter of 250 μm [21]. The size of the focused light spot is $\lambda_{in} f / \pi \omega_0 \approx 4$ μm , which is far smaller than the diameter of the SF; therefore, to increase the laser-induced RI modulation area, i.e., to increase the overlap integral between the RI modulation and coupling modes, a laser scanning exposure technique is adopted. As shown in Fig. 1(a), during the exposure process, the fiber moves along the X-axis at a constant speed; the moving speed is 0.1625 $\mu\text{m/s}$ and the total exposure time is approximately 25 min. To ensure the uniformity of the grating fringe distribution, the fiber is placed on a high-precision air-bearing translation stage.

To verify the RI modulation area induced by scanning exposure, we analysed the grating morphology in detail using selective chemical etching, because the RI modulation induced by the fs laser can increase the chemical etching speed [22]. Since it is difficult to etch the SF even after fs laser exposure, we inscribed a Bragg grating in a no-core silica fiber at the same time. These two types of FBGs were etched in an HF solution with a 4% volume concentration. A morphology characterization of the etched grating was conducted with a scanning electron microscope (SEM).

B. Coupling Methods

In the experiment, we utilize splicing coupling and micro-lens coupling methods to analyse the characteristic spectrum. The structure illustration and the microscopy image of the splicing method are shown in Fig. 1(b) and (c), respectively. The splicing between the SF and the silica multimode fiber (MMF) is made with a fusion splicer (FSU-975, Ericsson). The distance d between the polished end face of the SF and the grating is 15 cm, and the core and cladding diameters of the MMF are 62.5 μm and 125 μm , respectively. The coupling efficiency of this type of splicing structure is low, which leads to difficulties in observing Bragg resonance with low reflectivity. However, based on the spectrum measurement results reported hereinafter, this kind of simple splicing method is adequate for sensing measurements. The micro-lens coupling method shown in Fig. 1(d) can be employed to improve the coupling efficiency. The micro-lens is coated on the end face of the fiber by dipping in an RI matching gel [23]. This type of complex coupling method is mainly used to achieve and analyse more comprehensive and detailed high-order resonance spectra. In specific spectrum measurement process, we utilize the supercontinuum broadband light source (Superk Compact, NKT Photonics) to produce the light signal, which transmits to the SFBG through the silica MMF circulator. Then the reflection light transmits to the circulator again and is collected by the optical spectrum analyzer (OSA) (AQ6370B, Yokogawa) with a resolution of 0.02 nm, however, the transmission light is collected by the OSA directly. The above process realizes the monitoring and recording of reflection and transmission spectra, respectively.

III. THEORETICAL ANALYSIS

A single-crystal SF with a columnar structure is composed of Al_2O_3 material, which forms a step index RI multimode fiber with air cladding. The mode number transmitted in this kind of weak-guide fiber is affected by the SF diameter a , which can be expressed as $N \approx V^2/2$ [24]. Here, $V = (a\pi/\lambda) \cdot NA$ is the normalized frequency at wavelength λ , and NA is the numerical aperture. For the SF with a diameter of 250 μm selected in this work, the effective NA is equal to 0.12 and the RI (n_1) is equal to 1.746 [20]. At the 4th-order Bragg resonance (1454 nm), the mode number that can be transmitted is approximately 2100. According to $NA = \sqrt{n_1^2 - n_2^2}$ (n_2 is the RI of air cladding), the modes that can be transmitted are approximately 300000 in theory. Such numerous modes would make the spectrum of the Bragg resonance broad. Therefore, a theoretical analysis of the mode excitation and multimode resonance is important to understand the multimode transmission characteristics of the SF and the operation principle of the SFBG.

A. Multimode Excitation

For coupling between the silica fiber and the SF, we use the linear polarization mode approximation. Because of the rotationally symmetric structure of the silica fiber and the circular symmetry of the input light field, a fundamental mode light field $E(r, 0)$ that approximates a Gaussian beam will only excite a series of $\text{LP}_{0\mu}$ (or $\text{HE}_{0\mu}$) guided modes in the SF [25], [26]. These guided modes and radiation modes together form a group of orthogonal sets. Neglecting the radiation modes, the light field distribution at the initial position ($z = 0$) in the SF can be expressed as a series expansion of the guided modes:

$$E(r, \varphi, 0) = \sum_{\mu=1}^M c_{\mu} \Psi_{0\mu}(r, \varphi, 0) \quad (1)$$

in which $\Psi_{0\mu}(r, \varphi, z)$ is the electric field distribution of the $\text{LP}_{0\mu}$ guided mode and c_{μ} is the mode excitation coefficient, which can be determined from the overlap integral between $E(r, \varphi, 0)$ and $\Psi_{0\mu}(r, \varphi, 0)$:

$$c_{\mu} = \frac{\int_0^{2\pi} d\varphi \int_0^{\infty} E(r, \varphi, 0) \Psi_{0\mu}(r, \varphi, 0) r dr}{\int_0^{2\pi} d\varphi \int_0^{\infty} \Psi_{0\mu}(r, \varphi, 0) \Psi_{0\mu}(r, \varphi, 0) r dr} \quad (2)$$

After propagating along a distance of z within the SF section, the light field distribution can be expressed as follows:

$$E(r, \varphi, z) = \sum_{\mu=1}^M c_{\mu} \Psi_{0\mu}(r, \varphi, z) \exp(i\beta_{\mu} z) \quad (3)$$

in which $\beta_{\mu} = (2\pi/\lambda)n_{eff}^{\mu}$ is the propagation constant of the $\text{LP}_{0\mu}$ mode and n_{eff}^{μ} is the effective RI of the $\text{LP}_{0\mu}$ mode. In an actual theoretical simulation, the effect of the angular component φ can be ignored for the $\text{LP}_{0\mu}$ guided mode.

B. Multimode Bragg Resonance

When multiple excited transmission modes travel to the Bragg grating along the SF, their multimode resonance characteristics can be analysed by coupled mode theory [27], [28]. The modes

that satisfy the following phase-matching condition will be reflected:

$$\beta_{\nu} = \beta_{\mu} + m(2\pi/\Lambda), \text{ or } m\lambda_{\nu\mu} = (n_{eff}^{\mu} + n_{eff}^{\nu})\Lambda \quad (4)$$

in which Λ is the grating period and m is the resonance order. β_{μ} and β_{ν} are the propagation constants of the forward and backward guided modes and are of opposite sign. The coupling strength is determined by the overlap integral between the RI modulation and the interacting modes, i.e., the coupling coefficients between $\text{LP}_{0\mu}$ and $\text{LP}_{0\nu}$ modes [29], [30]. In general, the longitudinal coupling coefficient $K_{\nu\mu}^z$ is far smaller than the transverse coefficient $K_{\nu\mu}^t$ and can be ignored; $K_{\nu\mu}^t$ can be expressed as follows:

$$K_{\nu\mu}^t(z) = \frac{\omega}{4} \int_0^{2\pi} d\varphi \int_0^{\infty} \Delta\epsilon(r, z) e_{\nu}^t(r, \varphi, z) \cdot e_{\mu}^{t*}(r, \varphi, z) r dr \quad (5)$$

in which ω is the angular frequency. $\Delta\epsilon(r, z)$ is the perturbation to the permittivity, which is assumed to be independent of φ . When the effective RI change δn_{eff} is far less than n_{eff} , $\Delta\epsilon(r, z) \approx 2n_{eff}\delta n_{eff}(r, z)$. $e_{\mu}^t(r, \varphi, z)$ and $e_{\nu}^t(r, \varphi, z)$ are electric field distributions of the normalized unit power of $\text{LP}_{0\mu}$ and $\text{LP}_{0\nu}$, respectively. In the numerical simulation process, we only consider power coupling among the same modes.

IV. RESULTS AND DISCUSSION

A. Refractive Index Modulation

Illustrating the radial RI modulation area, the morphologies of the SFBG and no-core silica fiber Bragg gratings (NC-FBGs) etched by HF solution are shown in the left and right columns of Fig. 2, respectively, with etching times of 60 hr and 45 min. The arrows denote the laser beam direction. Because of the self-focusing effect of the ultrafast laser and the cylindrical lens effect of the fiber, the periodical RI modulation extends to the surface of the fiber [22]. Selective etching will occur from the surface to the inside. The morphology of the etched SFBG is shown in Fig. 2(a) and (b); obviously, the grating has almost no variation. A microscopy image of the SFBG is shown in Fig. 2(c), and the grating is uniformly distributed with a period of 1.665 μm . As shown in Fig. 2(d), the RI modulation area of the NC-FBG shows significant etching. Fig. 2(e) shows the cleavage morphology of the NC-FBG; the grating is uniformly distributed in the fiber with a stratiform morphology. A magnified image is shown in Fig. 2(f). According to the analysis of the corrosion trace of the end face, the radial RI modulation area exceeds 60%. Consequently, we infer that the SFBG should also have a similar RI modulation area, which is beneficial for increasing the coupling strength of the modes.

B. Spectral Characteristics

To evaluate the spectral characteristics of each order Bragg resonance in detail, we measure the spectrum with the micro-lens coupling method shown in Fig. 1(d); the achieved spectra are shown by black curves in Fig. 3. For the experimental conditions employed in this paper, the 4th- to 8th-order Bragg resonances are located at 1453 nm, 1166 nm, 973 nm, 836 nm,

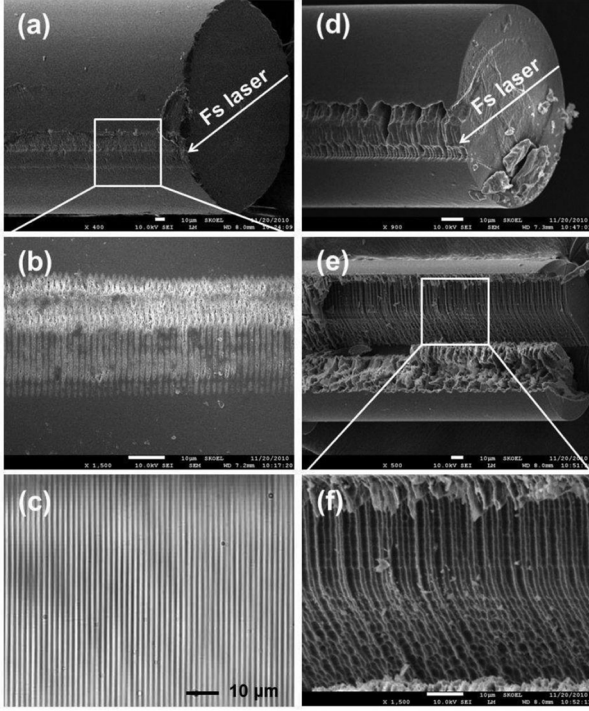


Fig. 2. (a) SEM image of the etched SFBG. (b) Magnified view of the surface damage area of the SFBG. (c) Microscopy image of the RI modulation of the SFBG. (d) SEM image of the etched NC-FBG. (e) Internal grating morphology of the stratiform NC-FBG. (f) Characteristics of the internal grating.

and 733 nm, respectively, which satisfy the phase-matching condition in (4). The multimode transmission leads to a wide resonance spectrum. Because the mode coupling of the low-order Bragg resonance is strong, the reflection and transmission peaks from the 4th to 6th order are strong; however, the reflection peaks of the 7th- and 8th-order resonances are weak. The large radial RI modulation area achieved by the scanning exposure results in a transmission amplitude of approximately 3.0 dB, as shown in Fig. 3(a). The transmission peak amplitude denotes the upper limit of the reflectivity, as it contains the net reflection and scattering loss from the Bragg grating. For comparison, we also show the resonance spectra obtained with the splicing coupling method as the red curve shown in Fig. 3. Due to the low coupling efficiency, only the resonance spectra from the 4th to 6th order are observed. However, the coupling efficiency is sufficient for sensing measurements based on the achieved resonance peak strength. In the sensing experiment, this simple splicing coupling method is adopted to monitor the spectrum variation.

C. Numerical Simulation

Following the theoretical analysis in Section II-B, we conduct numerical simulations on the multimode excitation of the SF and the multimode resonance of the SFBG. We employ the following suppositions and approximations: 1) The light field intensity of the fundamental mode input to the SF is taken as $E(r, 0) = 1$. 2) Only a series of guided modes $LP_{0\mu}$ (or $HE_{0\mu}$) is excited in the SF, and the angular component φ can be ignored. 3)

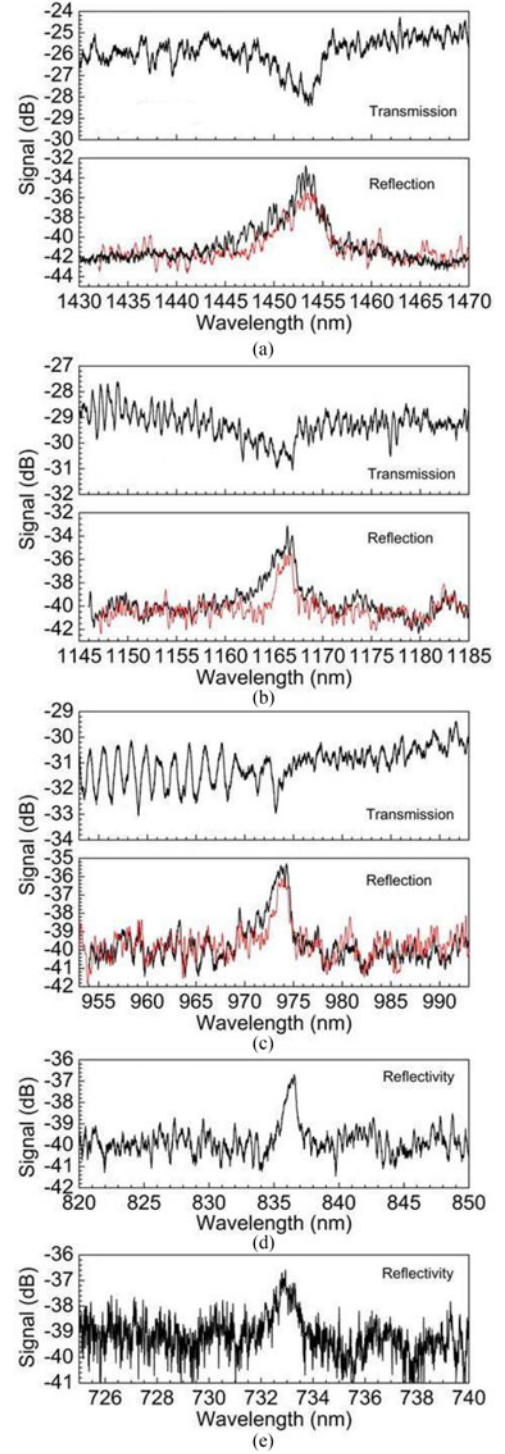


Fig. 3. (a)–(c) Reflection and transmission spectra of the 4th- to 6th-order Bragg resonances. (d)–(e) Reflection spectra of the 7th- and 8th-order Bragg resonances.

Mode coupling is only considered between a guided mode and its corresponding backward mode, i.e., $\beta_\nu = -\beta_\mu$, $n_{eff}^\nu = n_{eff}^\mu$, $e_\nu^\nu(r, \varphi, z) = e_\mu^\mu(r, \varphi, z)$. 4) The RI modulation range induced by the fs laser is assumed to cover the whole fiber cross-section. With these assumptions, we conduct a simulation of the power re-distribution of the excited modes. Fig. 4 shows the power

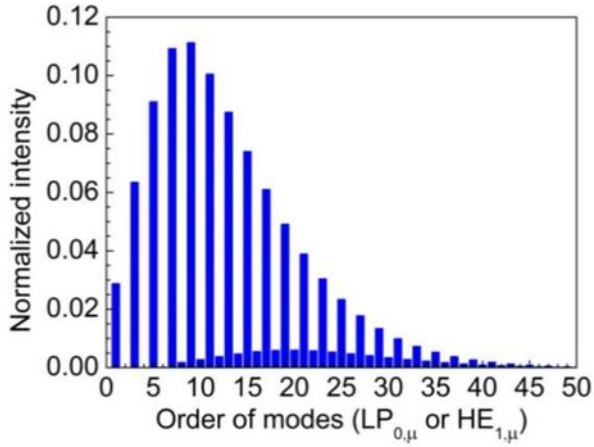


Fig. 4. Power distributions of the excited guided modes.

distributions of the first 50 ($\mu = 1, 2 \dots 50$) excited modes; as seen, more power is coupled to the odd-order modes. Moreover, since the electric field overlap integral between the fundamental mode of the silica fiber and LP_{09} mode is the highest, which means that the excitation coefficient of LP_{09} mode is the highest. Therefore, the allocated power of LP_{09} mode is higher than LP_{01} mode and other modes.

The excited guided modes suffer from the modulation of the Bragg grating, which will lead to self-coupling among the modes. Based on the coupled mode theory, for the 4th-order Bragg resonance, transmission resonance simulation results for different coupling strengths are shown in Fig. 5, where $K_{\nu\mu}^t$ is 0.0001, 0.0005, 0.0020, and 0.0035. In the situation of weak coupling, i.e., $K_{\nu\mu}^t \leq 0.0005$, the self-coupling resonances of each odd-order mode are independent, which is difficult to observe in the experiment because the unavoidable multimode interference existing in the SF leads to strong noise in the spectrum. With an increase in $K_{\nu\mu}^t$, the coupling strengthens and the resonance of each mode overlaps greatly, forming a wide resonance peak. The simulation result shown in Fig. 4(c) and the transmission spectrum shown in Fig. 3(a) match well. In the experiment, the coupling strength of the grating can be altered by controlling the laser intensity and the radial RI modulation area.

D. Sensing Characteristics and Discussion

Temperature and strain are important physical parameters in structural health monitoring; therefore, we studied the temperature and strain sensing characteristics of the SFBG. The wavelength shift ($\Delta\lambda_B^m$) of each order Bragg resonance could be seen as a function of temperature and strain; here, we only analysed the 4th- and 5th-order resonances, as shown in Fig. 6. Fig. 6(a) shows the temperature response of the SFBG from room temperature (20 °C) to 1690 °C and the 2nd-order polynomial fitting result. Each sampled data point was collected after the SFBG had been held at a constant temperature for 1 h. The temperature sensitivities of the 4th- and 5th-order Bragg resonances increase from 19.7 pm/°C and 17.4 pm/°C (room temperature) to 36.2 pm/°C and 32.5 pm/°C (1690 °C), respectively, with average values of 28.0 pm/°C and 25.0 pm/°C.

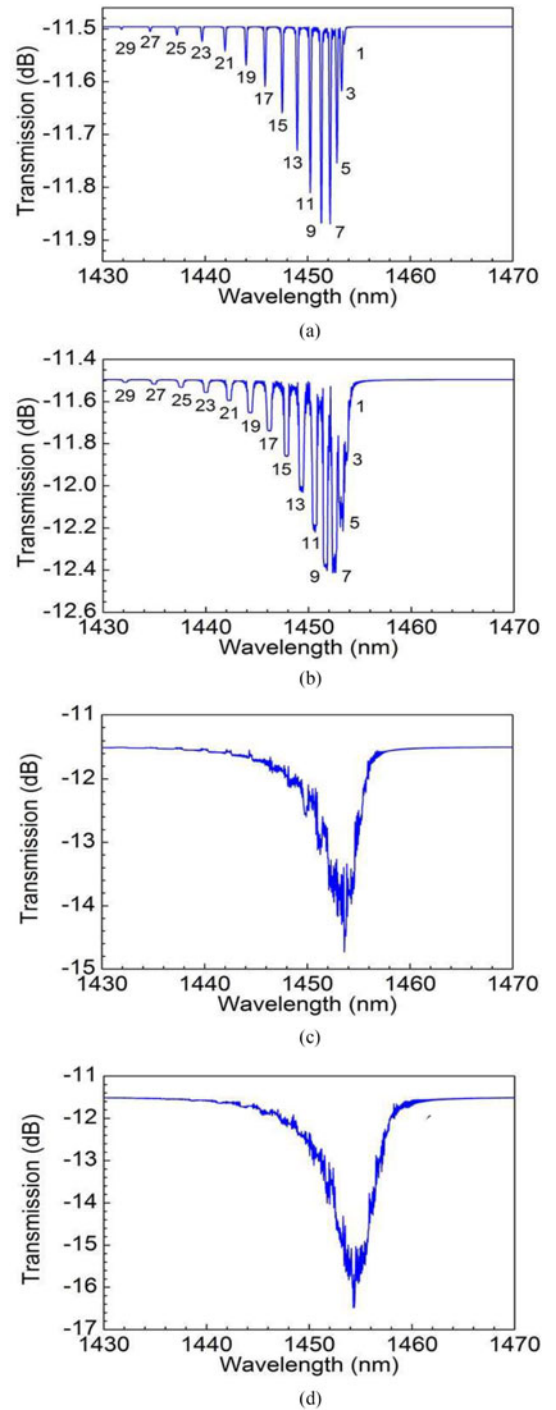


Fig. 5. Simulated transmission spectra, corresponding to coupling coefficients of 0.0001 (a), 0.0005 (b), 0.0020 (c), and 0.0035 (d).

The strain measurement was realized by applying axial stress to the SFBG (0 ~ 2.5 N). The applied axial strain can be calculated by the equation $\varepsilon = F/(\pi r^2 E)$, in which F is the axial stress, r is the fiber radius, and E is Young's modulus. Fig. 6(b) shows the relationship between the wavelength shift and axial strain of the 4th- and 5th-order resonance. The strain sensitivities are 1.39 pm/ $\mu\varepsilon$ and 1.00 pm/ $\mu\varepsilon$, respectively, based on linear fitting.

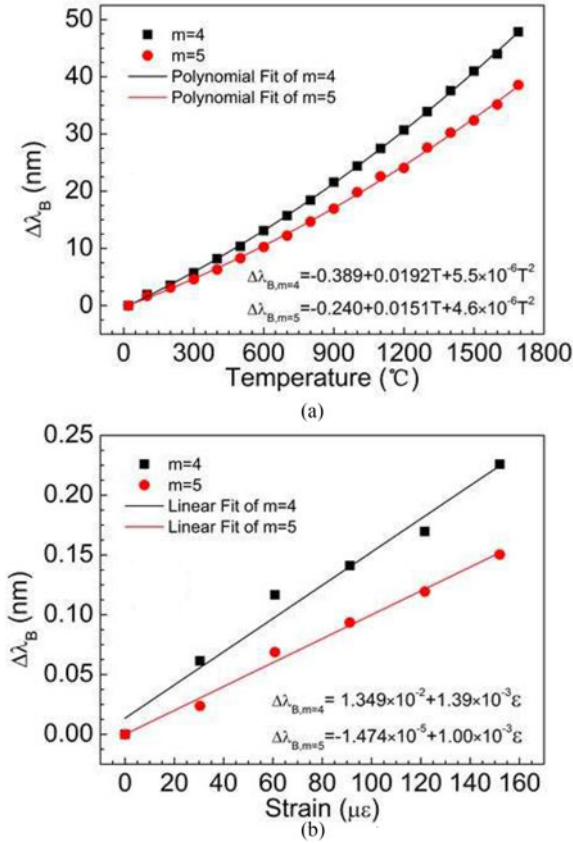


Fig. 6. Response characteristics of the 4th- and 5th-order Bragg resonances of the SFBG for temperature (a) and axial strain (b).

For the SFBG sensor, the resonance wavelength shifts caused by temperature and strain can be derived as $\Delta\lambda_B^m = \lambda_B^m (\alpha + \zeta) \Delta T + \lambda_B^m (1 - p_e) \Delta \epsilon$, in which ΔT and $\Delta \epsilon$ are the variations of temperature and strain, $\alpha = 7.15 \cdot 10^{-6} \text{ K}^{-1}$ and $\zeta = 12.6 \cdot 10^{-6} \text{ K}^{-1}$ are the thermal expansion coefficient and thermal optic coefficient of the c-axis sapphire (at 633 nm), and $p_e = 0.1277$ is the elastic optic coefficient [20]. For the 4th- and 5th-order resonances, the calculated temperature and strain sensitivities are 28.7 pm/ $^{\circ}\text{C}$ and 23.0 pm/ $^{\circ}\text{C}$ and 1.27 pm/ $\mu\epsilon$ and 1.02 pm/ $\mu\epsilon$, respectively, which match well with the experimental results.

In sensing applications of SFBGs in harsh environments, the cross-sensitivity problem is inevitable. For the 4th- and 5th-order Bragg resonances, the estimated cross-sensitivities of temperature and strain are 20.1 $\mu\epsilon/^{\circ}\text{C}$ and 25.0 $\mu\epsilon/^{\circ}\text{C}$ and 0.0496 $^{\circ}\text{C}/\mu\epsilon$ and 0.0400 $^{\circ}\text{C}/\mu\epsilon$, respectively. Here, the average temperature sensitivities are used. To study the cross-sensitivity problem of the SFBG at this stage, the blackbody radiation level of a SF can be used as a temperature reference, which has been analysed in detail in [20]. In the high-temperature measurement process, we also observed a background signal enhancement from the blackbody radiation. However, the use of this kind of modulation mechanism to solve the cross-sensitivity problem is limited to temperatures above 650 $^{\circ}\text{C}$, due to the strong dependence between the blackbody radiation signal intensity and temperature. Therefore, for the low-temperature range below

650 $^{\circ}\text{C}$ or for the whole temperature range, solutions to the cross-sensitivity problem are necessary for future SFBG structural health monitoring.

V. CONCLUSION

Aiming at the application of SFs in enhancing smart composite materials and embedded fiber sensors, we demonstrated the fabrication of a high-order Bragg grating with a large-diameter SF using an fs laser scanning exposure technique. A radial RI modulation area greater than 60% of the fiber cross-section was demonstrated, which resulted in strong mode coupling and a transmission resonance amplitude of approximately 3.0 dB. Multimode Bragg resonance spectra from the 4th order to 8th order were also observed. Based on numerical simulations of mode excitation and multimode resonance, the theoretical and experimental results matched well when the coupling coefficient was equal to 0.0020. In addition, we also studied the high-temperature and strain sensing characteristics of the SFBG and briefly discussed the temperature-strain cross-sensitivity.

REFERENCES

- [1] W.-K. R. K. Nubling and J. A. Harrington, "Optical properties of single-crystal sapphire fibers," *Appl. Opt.*, vol. 36, no. 24, pp. 5934–5940, Aug. 1997.
- [2] G. W. Tregay, P. R. Calabrese, P. L. Kaplin, and M. J. Finney, "Optical fiber sensor for temperature measurement from 600 to 1900 $^{\circ}\text{C}$ in gas turbine engines," *Proc. SPIE*, vol. 1589, pp. 38–47, Dec. 1991.
- [3] I. McKenzie and N. Karafolas, "Fiber-optic sensing in space structures: the experience of the European Space Agency," *Proc. SPIE*, vol. 5855, pp. 262–269, 2005.
- [4] G. J. de Villiers, J. Treurnicht, and R. T. Dobson, "In-core high temperature measurement using fiber-Bragg gratings for nuclear reactors," *Appl. Therm. Eng.*, vol. 38, pp. 143–150, May 2012.
- [5] W. Ecke, I. Latka, R. Willsch, A. Reutlinger, and R. Graue, "Fibre optic sensor network for spacecraft health monitoring," *Meas. Sci. Technol.*, vol. 12, no. 7, pp. 974–980, Jul. 2001.
- [6] R. D. Sante, "Fibre optic sensors for structural health monitoring of aircraft composite structures: Recent advances and applications," *Sensors*, vol. 15, no. 8, pp. 18666–18713, Jul. 2015.
- [7] N. Saheb and S. Mekid, "Fiber-embedded metallic materials: from sensing towards nervous behavior," *Materials*, vol. 8, pp. 7938–7961, Nov. 2015.
- [8] G. Zhou and L. M. Sim, "Damage detection and assessment in fibre-reinforced composite structures with embedded fibre optic sensors," *Smart Mater. Struct.*, vol. 11, no. 6, pp. 925–939, Oct. 2002.
- [9] D. E. Hajas, S. Kyrsta, S. Richter, J. Mayer, and J. M. Schneider, "Strength degradation mechanisms in h-BN/NiAl coated sapphire fibres with a reactive Hf or Y interlayer," *Mat. Sci. Eng. A*, vol. 491, pp. 207–213, Sep. 2008.
- [10] A. Ghazanfari, W. Li, M. C. Leu, Y. Zhuang, and J. Huang, "Advanced ceramic components with embedded sapphire optical fiber sensors for high temperature applications," *Mater. Des.*, vol. 112, pp. 197–206, Dec. 2016.
- [11] K. Wood, T. Brown, R. Rogowski, and B. Jensen, "Fiber optic sensors for health monitoring of morphing airframes: I. Bragg grating strain and temperature sensor," *Smart Mater. Struct.*, vol. 9, pp. 163–169, 2000.
- [12] S. J. Mihailov, D. Grobncic, C. W. Smelser, P. Lu, R. B. Walker, and H. Ding, "Bragg grating inscription in various optical fibers with femtosecond infrared lasers and a phase mask," *Opt. Mater. Express*, vol. 1, no. 4, pp. 754–765, Aug. 2011.
- [13] J. Thomas, C. Voigtländer, R. G. Becker, D. Richter, A. Tünnermann, and S. Nolte, "Femtosecond pulse written fiber gratings: a new avenue to integrated fiber technology," *Laser Photon. Rev.*, vol. 6, no. 6, pp. 709–723, Nov. 2012.
- [14] M. Malinauskas *et al.*, "Ultrafast laser processing of materials: From science to industry," *Light, Sci. Appl.*, vol. 5, Aug. 2016, Art. no. e16133.
- [15] D. Grobncic, S. J. Mihailov, C. W. Smelser, and H. Ding, "Sapphire fiber Bragg grating sensor made using femtosecond laser radiation for ultrahigh temperature applications," *IEEE Photon. Technol. Lett.*, vol. 16, no. 11, pp. 2505–2507, Nov. 2004.

- [16] T. Elsmann, T. Habisreuther, A. Graf, M. Rothhardt, and H. Bartelt, "Inscription of first-order sapphire Bragg gratings using 400 nm femtosecond laser radiation," *Opt. Express*, vol. 21, no. 4, pp. 4591–4597, Feb. 2013.
- [17] D. Grobnić, S. J. Mihailov, H. Ding, F. Bilodeau, and C. W. Smelser, "Single and low order mode interrogation of a multimode sapphire fibre Bragg grating sensor with tapered fibres," *Meas. Sci. Technol.*, vol. 17, no. 5, pp. 980–984, Apr. 2006.
- [18] M. Busch, W. Ecke, I. Latka, D. Fischer, R. Willsch, and H. Bartelt, "Inscription and characterization of Bragg gratings in single-crystal sapphire optical fibres for high-temperature sensor applications," *Meas. Sci. Technol.*, vol. 20, no. 11, Oct. 2009, Art. no. 115301.
- [19] C. Zhan, J. H. Kim, J. Lee, S. Yin, P. Ruffin, and C. Luo, "High temperature sensing using higher-order-mode rejected sapphire-crystal fiber gratings," *Proc. SPIE*, vol. 6698, 2007, Art. no. 66980F.
- [20] S. J. Mihailov, D. Grobnić, and C. W. Smelser, "High-temperature multiparameter sensor based on sapphire fiber Bragg gratings," *Opt. Lett.*, vol. 35, no. 16, pp. 2810–2812, Aug. 2010.
- [21] [Online]. Available: http://photran.com/photran_pages/product_pages/optical_fiber.html
- [22] R. Yang, Y. S. Yu, C. Chen, Q. D. Chen, and H. B. Sun, "Rapid fabrication of microhole array structured optical fibers," *Opt. Lett.*, vol. 36, no. 19, pp. 3879–3881, Oct. 2011.
- [23] X. Y. Zhang *et al.*, "Miniature end-capped fiber sensor for refractive index and temperature measurement," *IEEE Photon. Technol. Lett.*, vol. 26, no. 1, pp. 7–10, Jan. 2014.
- [24] D. Gloge, "Weakly guiding fibers," *Appl. Opt.*, vol. 10, no. 10, pp. 2252–2258, Oct. 1971.
- [25] Q. Wang, G. Farrell, and W. Yan, "Investigation on single-mode-multimode-single-mode fiber structure," *J. Lightw. Technol.*, vol. 26, no. 5, pp. 512–519, Mar. 2008.
- [26] T. L. Wu and H. W. Chang, "Guiding mode expansion of a TE and TM transverse-mode integral equation for dielectric slab waveguides with an abrupt termination," *J. Opt. Soc. Amer. A*, vol. 18, no. 11, pp. 2823–2832, Nov. 2001.
- [27] T. Erdogan, "Cladding-mode resonances in short- and long- period fibre grating filters," *J. Opt. Soc. Amer. A*, vol. 14, no. 8, pp. 1760–1773, 1997.
- [28] T. Erdogan, "Fiber grating spectra," *J. Lightw. Technol.*, vol. 15, no. 8, pp. 1277–1294, Aug. 1997.
- [29] C. Lu and Y. Cui, "Fiber Bragg grating spectra in multimode optical fibers," *J. Lightw. Technol.*, vol. 24, no. 1, pp. 598–604, Jan. 2006.
- [30] M. J. Schmid and M. S. Muller, "Measuring Bragg gratings in multimode optical fibers," *Opt. Exp.*, vol. 23, no. 6, pp. 8087–8094, Mar. 2015.

Chao Chen received the B.S., M.S., and Ph.D. degrees in electronics science and technology from Jilin University, Changchun, China, in 2005, 2010, and 2014, respectively. He is currently an Assistant Professor with the State Key Laboratory of Luminescence and Application, Changchun Institute of Optics, Fine Mechanics and Physics, Chinese Academy of Sciences, Changchun. His current research interests include optical devices and sensors, micro-nano fabrication, and narrow linewidth semiconductor laser.

Xuan-Yu Zhang received the B.S. degree from Jilin University, China, in 2012. He is currently working toward the Ph.D. degree in physical electronics at Jilin University. His current research interests include theory of fiber gratings and fabrication of fiber gratings and the interaction of femtosecond laser and material.

Yong-Sen Yu received the M.S. degree in electronics from Changchun University of Science and Technology, Changchun, China, in 2000, and the Ph.D. degree in microelectronics and solid electronics from Jilin University, Changchun, China, in 2005. In 2009, he worked as an Associate Professor in State Key Laboratory of Integrated Optoelectronics, Jilin University, Changchun, China. His current research interests include laser microfabrication, fiber gratings, and fiber optic sensor.

Wei-hua Wei, biography not available at the time of publication.

Qi Guo, biography not available at the time of publication.

Li Qin received the B.S. and M.S. degrees in semiconductor physics and the Ph.D. degree in microelectronics and solid electronics from Jilin University, Changchun, China. She was a Post-Doctoral Researcher with the Changchun Institute of Optics, Fine Mechanics and Physics, Chinese Academy of Sciences, Changchun, China, from 2000 to 2002. She became a Professor in September 2008. She has authored and coauthored more than 40 refereed journal and conference papers. Her current research interests include high power vertical-cavity surface-emitting lasers, edge-emitting semiconductor lasers, and distributed feedback lasers.

Yong-Qiang Ning received the M.S. degree in semiconductor materials from Beijing General Research Institute for Nonferrous Metals, Beijing, China, in 1990, and the Ph.D. degree in condensed matter physics from the Changchun Institute of Optics, Fine Mechanics and Physics, Chinese Academy of Sciences, Changchun, China, in 1999. He was a Visiting Scholar with Cardiff University, Wales, U.K., from 1999 to 2000. He is currently a Professor with the Changchun Institute of Optics. He has authored and co-authored more than 60 refereed journal and conference papers. His current research interests include the design of high power vertical-cavity surface-emitting lasers, III–V related material MOCVD growth, and diode laser applications.

Li-Jun Wang received the M.S. degree from the College of Electrical Science, Jilin University, Changchun, China, in 1973. He was a Research Fellow with Jilin University until 1986. He joined the Changchun Institute of Optics, Fine Mechanics and Physics, Chinese Academy of Sciences, Changchun, China. From 1988 to 1989, he was with Swiss Postal Telegraph and Telephone agency, Bern, Switzerland. He was a Senior Visiting Scholar with Northwestern University, Chicago, IL, USA, from 1993 to 1995. From 1995, he was a Leading Professor with the Changchun Institute of Optics. He was elected an academician of the Chinese Academy of Sciences in 2013. He has more than 30 years of experience in the research of the semiconductor laser theory, technology, and applications. He hosted and participated in 15 national and ministerial important projects, achieved three international leading results, authorized 23 Chinese patents, published more than 300 papers, and three academic books.

Hong-Bo Sun (F'17) received the B.S. and Ph.D. degrees in electronics from Jilin University, Changchun, China, in 1992 and 1996, respectively. He was a Postdoctoral Researcher with the University of Tokushima, Japan, from 1996 to 2000, and then an Assistant Professor with the Department of Applied Physics, Osaka University, Japan. In 2005, he was promoted to a Full Professor (Changjiang Scholar) with Jilin University. In September 2017, he moved to Tsinghua University. He has authored or coauthored more than 350 scientific papers, which have been cited more than 12 000 times, with an H-factor of 56. His research interests include ultrafast optoelectronics, particularly on laser nanofabrication and ultrafast spectroscopy. In 2017, he became an OSA Fellow.